Chemical Engineering Science 66 (2011) 6028–6038

Contents lists available at SciVerse ScienceDirect

Chemical Engineering Science

journal homepage: www.elsevier.com/locate/ces

CFD modeling of gas flow in porous medium and catalytic coupling reaction from carbon monoxide to diethyl oxalate in fixed-bed reactors

Xi Gao, Ya-Ping Zhu, Zheng-hong Luo*

Department of Chemical and Biochemical Engineering, College of Chemistry and Chemical Engineering, Xiamen University, Xiamen 361005, PR China

ARTICLE INFO

Article history:
Received 4 April 2011
Received in revised form
16 July 2011
Accepted 15 August 2011
Available online 22 August 2011

Keywords:
Porous medium
Multiphase reactors
Packed bed
Mathematical modeling
Catalytic coupling reaction from carbon monoxide to diethyl oxalate
CFD

ABSTRACT

A comprehensive two-dimensional heterogeneous reactor model was developed to simulate the flow behavior and catalytic coupling reaction of carbon monoxide (CO)–diethyl oxalate (DEO) in a fixed-bed reactor. The two-temperature porous medium model, which was revised from a one-temperature porous medium model, as well as one equation turbulent model, and exponent-function kinetic model was constructed for the turbulent velocity scale comparing with laminar flow and simulation of the catalytic coupling reaction. The simulation results were in good agreement with the actual data collected from certain pilot-plant fixed bed reactors in China. Based on the validated approach and models, the distributions of reaction parameters such as temperature and component concentrations in the reactor were analyzed. The simulations were then carried out to understand the effects of operating conditions on the reactor performance which showed that the conduction oil temperature in the reactor jacket and the CO concentration are the key impact factors for the reactor performance.

1. Introduction

As one of the most important alcoholic compounds, ethylene glycol (EG) is widely used, particularly in the field of polyester, synthetic fiber and paint industry, etc. (Eugene and Andre, 2001; Shoaeifar et al., 2007). Recently, a green process for the preparation of EG independent of petroleum, as described in Scheme 1, was developed based on coal (Meng, 2003; Li et al., 2005; Xu et al., 2008a, b). It was first industrialized in China in 2009 (Qian, 2009). This green process is one of the promising methods to convert coal to high-value chemicals (UOPLLC, 2002). Its key part is the coupling reaction, which is shown in

$$2CO+2EtONO \xrightarrow{\text{Coupling reaction}} (COOEt)_2+2NO. \quad (1)$$

Eq. (1) shows that diethyl oxalate ($(COOEt)_2$, DEO) is synthesized through the coupling reaction between carbon monoxide (CO) and ethyl nitrite (EtONO, EN) over supported metal catalyst.

The coupling reaction attracted great interests (Bartley and Charleston, 1987; Chatterjee et al., 2001; Gao et al., 2005; Ji et al., 2009; Le Gall et al., 2001; Shiomi et al., 1989; Wu et al., 2003; Xiao et al., 2000; Xu et al., 1995; Zhang et al., 1995). Most of them focused on the coupling reaction catalyst (Bartley and Charleston, 1987; Shiomi et al., 1989; Wu et al., 2003; Xu et al., 1995; Zhang et al., 1995) and mechanism (Chatterjee et al., 2001; Gao et al., 2005; Ji et al., 2009; Le Gall et al., 2001; Xiao et al., 2000). There are still few studies on the coupling reactors, particularly about the fluid dynamics in these reactors, which can be used to evaluate the reactor performance. Recently, Xu et al. (2008a, b) established a fixed-bed reactor model for the catalytic coupling reaction of CO–DEO. In their study, the gas concentration, temperature and pressure profiles along the axial direction inside the reactor were obtained. However, the usual assumption to model fixed-bed reactors of plug flow was still retained. In addition, Wang et al. (2000) developed a two-dimensional fixed-bed reactor model of coupling reactor of CO–DEO by using advanced software tools, Aspen and Pro-II. However, the special hot spots and their positions cannot be obtained accurately via their reactor models. In addition, the hot spot temperature obtained via the reactor model with ignoring any side reactions cannot reflect the practical situation very well. In practice, the above reactor performance including hot spot information can be predicted via modern computational fluid dynamics (CFD) model. On the other hand, the reactors mentioned above are both fixed-bed reactors, which play a very important part in the chemical industry (Nijemeisland and Dixon, 2004a). Some reactor models were constructed to examine reactor operation parameters. Unfortunately, in present open reports (Bub et al., 1980; Jess et al., 1999), the usual approach to model fixed bed reactors assumes plug flow and effective transport mechanisms. Recent works (Calis et al., 2001; Jiang et al., 2001) suggest that the better predictions of the

* Corresponding author. Tel.: +86 592 2187190; fax: +86 592 2187231.
E-mail address: luozh@xmu.edu.cn (Z.-h. Luo).

0009-2509/$ - see front matter © 2011 Elsevier Ltd. All rights reserved.
doi:10.1016/j.ces.2011.08.031

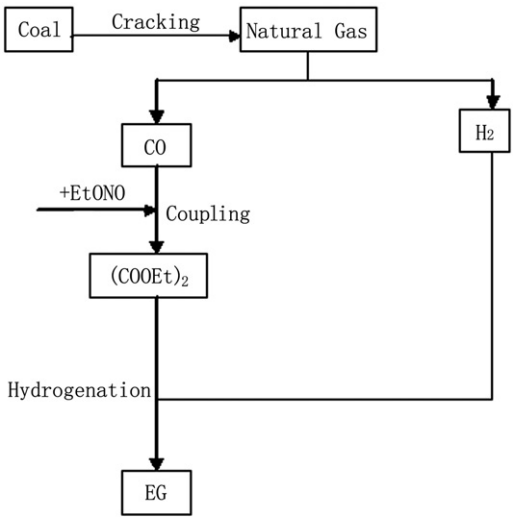

Scheme 1. A green process for the preparation of EG independent of petroleum.

reactor performance can be obtained for slim tubes if the radial variation of the axial flow component is included. However, effective parameters need to be estimated. The good predictions of the measured reactor performance profiles can only be obtained if an effective viscosity is incorporated.

As described above, the modern CFD model and the exponential growth of computer power are bringing simulations of fixed-bed flow into reality. It is now feasible to obtain detailed flow fields in fixed beds. Furthermore, the CFD is an emerging technique and holds great potential in providing detailed information of the complex fluid dynamics (Ding and Gidspow, 1990; Nijemeisland and Dixon, 2001; Tian et al., 2007a,b). Up to now, considerable attention has been devoted to the application of CFD in fixed-bed reactors (Eu Toit et al., 2006; Guardo et al., 2004; 2005; 2006; Lan et al., 2009; Lopes and Quinta-Ferreira, 2010a, b; Jafari et al., 2008; Jakobsen et al., 2002; Natarajan et al., 2005; Nijemeisland et al., 2004b; Nikačević et al., 2009; Taskin and Dixon, 2008). For instance, Nijemeisland and Dixon (2004a) studied the relationship between the local flow field and the local wall heat flux in a packed bed of spheres. In their work, the CFD was used as a tool to obtain the detailed velocity and temperature fields, when gas flow through a periodic wall segment test cell. Guardo et al. (2005) used the CFD as a simulation tool based on the Eulerian–Eulerian approach to obtain a more detailed view of the fluid flow and heat transfer mechanisms in fixed-bed reactors. This study presented a comparison between the performance in flow and heat transfer estimation of five different RANS turbulence models in a fixed-bed. In practice, most of the early modeling efforts in this field are regarding the fluid flow and heat transfer in gas–solid two-phase fixed-bed reactors. According to the best knowledge of us, so far, there was no open report regarding the application of CFD to the fixed-bed for the catalytic coupling reaction of CO–DEO. On the other hand, generally, due to the complexity of flow shapes in fixed-bed reactors, two CFD methods were applied to simulate the flow in fixed-bed reactors in the past. One handles the fixed-bed reactor as a porous medium or applies the assumption of a quasi-homogeneous reactor model (Jakobsen et al., 2002). Therefore, the reactions occurring in the reactor can be handled as a source item of the continuity equations. Using the method, one cannot obtain the micro-mechanism of liquid flow and transportation. The other solves directly the governing equations of liquid flow and transportation in complex pipelines, which does not simplify the flow shapes and the governing equations. Therefore, by using the direct solution method, a precise and microcosmic fluid flow field in the fixed-bed reactor can be obtained. However, this method needs complex computation meshes and boundary conditions (Calis et al., 2001; Nijemeisland and Dixon, 2004a; Petre et al., 2003).

In this work, based on the first CFD method mentioned above, a comprehensive two-dimensional heterogeneous CFD reactor model incorporating an exponent-function reaction kinetic model is applied to study the flow behavior and catalytic coupling reaction of CO–DEO in a fixed-bed reactor. A one-equation turbulent model suggested by Spalart and Allmaras (1992) is used for the turbulent velocity scale in the fixed-bed reactor. The solid energy equation and heat transfer equation are added into the porous medium model, thus the old one-temperature model is changed into two-temperature model. The CFD model is validated with the actual data collected from certain pilot-plant fixed bed-reactor (Xu et al., 2010) and some reaction parameter distributions in the reactor are also obtained via the above model.

2. Simulation of fixed-bed reactor and coupling reaction

Since Li et al. (2005) and Xu et al. (2010) have experimentally investigated the coupling reaction of CO–DEO in a fixed-bed reactor, the fixed-bed reactor described in their work (Li, et al., 2005; Xu et al., 2010) is selected as the object of our simulation. Referring to reference (Xu et al., 2010), the selected reactor has an inner diameter of 0.027 m and a length of 3 m. The reactor can be divided into three zones. Zone I and Zone III are used for preheating the feed gas and cooling the products, respectively. Zone II is in the middle section of the reactor where reactions occur. More detailed information regarding the fixed-bed reactor configurations is provided in Fig. 2.

On the other hand, as described earlier, the coupling reaction takes place over the supported metal catalyst in a fixed-bed reactor where the spheric catalyst particles of the same size are filled along the axis direction. The gaseous EN and CO are continuously fed into the reactor, and react over the solid catalyst particles to produce gaseous DEO and by-products. Therefore, the reacting system can be considered as a gas–solid two-phase system.

3. CFD model for the fixed-bed reactor

In order to make the simulation meet the demand of engineering, the catalyst particles in the bed are assumed as a continuous porous medium, which in CFD is modeled as a fluid region with extra terms in the momentum balance to allow for additional resistance to flow. However, the default solution of energy equation for the porous medium is based on one-temperature model in FLUENT 6.3.26, giving only an effective thermal conductivity for the porous region. It suggests that the temperature of solid phase equals that of gas phase due to the local thermal equilibrium between the gas–solid two phases. Obviously, it does not accord with the practical reactor. Therefore, the solid energy and heat transfer equations are added into the porous medium model, thus the old one-temperature porous medium model is changed into two-temperature porous medium model.

Moreover, due to the complexity of the fluid flow in porous medium, the turbulent model is thoroughly discussed and simplified in the section. The detailed equations are presented in the following sections.

Table 1
Main governing equations of the two-temperature porous medium model.

Gas phase continuity equation:
$\nabla\cdot(\phi\rho_g\vec{v})=0$
Gas phase momentum equation:
$\nabla\cdot(\phi\rho_g\vec{v}\vec{v})=-\phi\nabla p+\nabla\cdot\phi\bar{\bar{\tau}}+\phi\rho_g\vec{g}-\vec{S}$
Gas phase equation of state:
$p=\rho_g RT_g$
Gas phase stress–strain tensor:
$\bar{\bar{\tau}}=\mu_g\left[(\nabla+\nabla\vec{v}^{\,T})-\frac{2}{3}\nabla\cdot\vec{v}\bar{\bar{I}}\right]$
Gas–solid momentum exchange rate (Ergun, 1952):
$\vec{S}=150\frac{(1-\phi)^2\mu_g}{d_p^2\phi^2}\vec{v}+1.75\frac{\rho_g(1-\phi)|\vec{v}|}{d_p\phi}\vec{v}$
Species conservation equation:
$\nabla\cdot(\phi\rho_g\vec{v}Y_i)=-\phi\nabla\cdot\vec{J}_i+R_i, i\in[1,N_r]$
Where, $\vec{J}_i=-\left(\rho_g D_{i,m}+\frac{\mu_t}{Sc_t}\right)\nabla Y_i$,
Mass rate of reaction:
$R_i=M_{w,i}\sum_{r=1}^{N_r}\left[(v''_{i,r}-v'_{i,r})\left(k_{f,r}\prod_{j=1}^{N_r}[C_{j,r}]^{(\eta'_{j,r}+\eta''_{j,r})}\right)\right]$
Gas-phase energy equation:
$\nabla\cdot[\phi\vec{v}(\rho_g E_g+p)]=\phi\nabla\cdot\left[k_g\nabla T_g-\left(\sum_{i=1}^{N_r}h_i\vec{J}_i\right)+\bar{\bar{\tau}}\cdot\vec{v}\right]+h_v(T_s-T_g)$
Solid-phase energy equation:
$0=\nabla\cdot((1-\phi)k_s\nabla T_s)-h_v(T_s-T_g)$
Heat transfer coefficient between gas and solid phases Wakao and Kaguei (1982), Henneke and Ellzey (1999)
$h_v=Nu_v k_g/d_p^2$
where, $Nu_v=2+1.1\mathrm{Pr}^{1/3}\mathrm{Re}^{0.6}$,
$\mathrm{Pr}=C_p\mu_g/k_g$,
$\mathrm{Re}=\rho_g v\phi D_b/\mu_g$.

3.1. Governing equations

Since there are solid and fluid phases in the porous medium, the flow is influenced by the solid matrix, which occupies space and extracts energy from the reaction zone. It is assumed that the solid is chemically inert. The main governing equations of the two-temperature porous medium model have been showing in Table 1.

3.2. Turbulence model

Using CFD as a simulation tool, together with the resolution of Reynolds averaged transport equations and also a simplified turbulence model (Guardo et al., 2005), allows us to obtain a more detailed view of the fluid flow and heat transfer mechanisms in fixed-bed reactors.

In the porous medium, with the increase of the gas Reynolds numbers (*Re*), the fluid flow can change from laminar flow to turbulence. In the present study, the average flow rate of fluid in the porous medium is about 0.25–2.0 m/s. The value of *Re* for porous medium is about 19–151 and the value of *Re* for the pipe is about 47–376. Thus, the fluid flow in the porous medium is in the transition flow range. In addition, Guardo et al. (2004) simulated the fluid flow and heat transfer in a nonregular packing bed. Their results showed that a laminar solution overestimates the value of heat transfer coefficient in the turbulent flow zone, and turbulent solutions tend to underestimate the value of the coefficient in the laminar transition zone. Guardo et al. (2005) further investigated the influence of the turbulence model in CFD modeling of wall-to-fluid heat transfer on packed beds. In Guardo et al.'s work (2005), five different RANS turbulence models including the Spalart–Allmaras model (one-eqaution model) (Coussirat, 2001) were selected. Results obtained from the Spalart–Allmaras turbulence model showed better agreement than the two-equation RANS models in their work. This could be explained by the fact that the Spalart–Allmaras model uses a coupling between wall and damping functions in the near-wall treatment, which does not include additional diffusion or dissipation terms in its formulation and does not present the stagnation point anomaly. On the contrary, for the two-equation RANS models including the $k-\varepsilon$ models (Durbin and Petterson, 2001; Launder and Spalding, 1974), misestimating of factors such as the ε, k or ν^T can lead to differences in flow. Consequently, temperature profiles can be miscalculated in heat transfer parameters. Therefore, the Spalart–Allmaras model could be a good tool for these kinds of flows in the fixed-bed because the y^+ problem is solved automatically (Guardo et al. 2005). Accordingly, since the fluid flow in the porous medium is at the status of the transition flow, simulations using the laminar flow and the Spalart–Allmaras turbulent flow are compared in the following work. The transported variable in the Spalart–Allmaras model, $\tilde{\nu}$, is identical to the turbulent kinematic viscosity except in the near-wall (viscous-affected) region. The transport equation for $\tilde{\nu}$ is (Spalart and Allmaras, 1992)

$$\frac{\partial}{\partial x_i}(\rho_g\tilde{\nu}v_i)=G_\nu+\frac{1}{\sigma_{\tilde{\nu}}}\left[\frac{\partial}{\partial x_i}\left\{\left(\mu_g+\rho_g\tilde{\nu}\right)\frac{\partial}{\partial x_j}\right\}+C_{b2}\rho_g\left(\frac{\partial\tilde{\nu}}{\partial x_j}\right)^2\right]-Y_\nu. \quad (2)$$

3.3. Reaction kinetic model

With the fluid flow in the fixed-bed reactor, the reaction kinetic model of the coupling reaction incorporated into the above CFD model. Therefore, their kinetics is also applied in this study as described below

The main reaction equations are listed below

$$2\mathrm{CO}+2\mathrm{EtONO}\rightarrow(\mathrm{COOEt})_2+2\mathrm{NO}, \quad (3)$$

$$\mathrm{CO}+2\mathrm{EtONO}\rightarrow(C_2H_5O)_2\mathrm{CO}+2\mathrm{NO}, \quad (4)$$

$$2EtONO \rightarrow C_2H_5OH + CH_3CHO + 2NO. \quad (5)$$

where, C_2H_5OH and CH_3CHO are ethanol and acetaldehyde, respectively. The kinetic equations corresponding to the above reaction equations are listed in Table 2 (Li et al., 2005). In this work, the used reaction kinetics of the catalytic coupling reaction of CO–DEO was derived from an experiment in a continuous flow fixed-bed integral-type reactor with a 16 mm internal diameter and a 15 mm length of catalyst bed. The experiment was carried out in the presence of ethyl nitrite over supported palladium catalyst in gaseous phase at the optimum CO coupling reaction conditions of temperature 383–403 K, space velocity 0.146–0.292 mol(g h), EN mole concentration 5–15% and CO mole concentration 20–35% at atmospheric pressure. Further details of the experiment are reported elsewhere (Li et al., 2005).

3.4. Boundary conditions

At the inlet, the velocity inlet was specified. The velocity, temperature, components, turbulent kinetic energy and its dissipation rate of the reactor inlet can be calculated based on the boundary conditions of the reactor inlet. At the outlet, the pressure outlet was specified. Furthermore, for the inner wall of the reactor, the fluids are assumed to obey the no slip boundary condition at the wall.

On the other hand, the coupling reaction is a highly exothermic reaction, and the heat must be removed from the reactor as soon as possible. In practice, there are jacket wrapped outside the reactor. Most reaction heat can be removed via heating the oil in the jacket. Therefore, the boundary condition for the reactor follows the convection heat-transfer equations shown in Eqs. (6)–(7) (Gao et al., 2010; Launder and Spalding, 1974)

$$q = h_{gc}(T_g - T_c), \quad (6)$$

$$\frac{1}{h_{gc}} = \frac{1}{\alpha_g} + \frac{b}{\lambda}\frac{A_i}{A_m} + \frac{1}{\alpha_c}\frac{A_i}{A_O}. \quad (7)$$

Table 2
The kinetics parameters of reaction system (Li et al. 2005).

Reactions	Kinetic expression	Pre-exponential factor	Active energy/ kJ/kmol	a	b
(1)	$r_1 = A_1 e^{(-E_1/RT_g)} y_{co}^a y_{en}^b$	2.7551×10^4	4.4623×10^4	0.49	0.40
(2)	$r_2 = A_2 e^{(-E_2/RT_g)} y_{co}^a y_{en}^b$	1.085×10^2	4.6673×10^4	1.14	1.22
(3)	$r_3 = A_3 e^{(-E_3/RT_g)} y_{co}^a y_{en}^b$	2.1832×10^4	4.6313×10^4	0	1.33

4. Simulations

4.1. CFD modeling method

The equations above were solved by the commercial CFD code FLUENT 6.3.26 (Ansys Inc., US) in double precision mode. The governing equations are discretized in a non-uniform structural mesh by a finite volume method. Grid independency for some mesh points and finally a 300×30 non-uniform mesh is selected. Diffusive fluxes were discretized using a central difference scheme and convective fluxes are evaluated using the differed correction scheme. Pressure and the velocity are coupled by the SIMPLE algorithm.

In order to simulate the practical case, the results of the flow field without the reaction at the steady-state are obtained first. Then the coupling reaction is further added into the flow field, simultaneously. The gas and solid temperatures in the porous medium are both set as a preheating-value (370 K). For the CFD simulations, the sub-relaxation iteration method is used to ensure the simulations convergence. Furthermore, the simulations were executed in a 2.83 GHz Pentium 4 CPU with 4 GB of RAM.

4.2. Model parameters

The actual data depend on the range of parameter values presented in equations listed in Table 1. Most of the parameters are directly linked to the properties of the gas and solid phases. Some parameters are reaction kinetic and heat transfer parameters. All of parameter values used in this work are listed in Tables 2–4. If no specific description, the same parameters are also used for the following simulation.

5. Results and discussion

5.1. Grid independency

No numerical simulation is complete without a study of grid-size dependence. To confirm that the CFD results are independent of the mesh size, the simulations of the system with 5×50, 10×100, 20×200, 30×300 and 40×400 grids (radial $\times$ axial) are performed feeding cold gas mixture. Fig. 1 shows the pressure drop at five mesh resolutions. It can be seen that all simulations predict almost the same pressure drop. Relative to the coarser mesh, the fine mesh (40×400) case and medium mesh (30×300) case capture the more real pressure drop along the reactor. Moreover, the medium and fine mesh cases obtain similar pressure drop, which indicates that the mesh size of 30×300 is sufficiently fine for providing reasonably mesh independent results. Therefore, the mesh size of 30×300 is selected as a base case and applied in the rest of the article.

Table 3
The thermodynamic data of the components in the reaction system (Meng, 2003).

Components	Phase	$\Delta H_{f,298}$ kj mol^{-1}	$\Delta G_{f,298}$ kj mol1^{-1} K^{-1}	C_P(j mol^{-1} K^{-1}) $= A + B \cdot T + C \cdot T^2 + D \cdot T^3$			
				A	$B \times 10^2$	$C \times 10^5$	$D \times 10^8$
CO	g	−110.53	−137.15	27.487	0.4248	0.2509	−0.1244
NO	g	90.37	86.69	29.199	−0.0780	0.9929	−0.4346
C_2H_5OH	g	−234.01	−167.99	6.7318	23.153	−12.116	2.4935
CH_2CHO	g	−166.19	−133.76	13.546	16.056	−7.4281	1.2669
EN	g	−104.25	9.42	6.5618	29.315	−16.311	3.2400
DEO	g	−745.5	−623.49	123.59	193.34	−66.506	0.1321
DEC	g	−625.83	−441.37	74.690	14.041	57.591	64.001
N_2	g	0	191.50	1116.071	−48.607	96	41.821

5.2. Model verification

Because the CFD methodology is not specifically designed for application in the catalytic coupling fixed-bed reactor, it is necessary to verify whether the simulated results are valid. Although the CFD code is based on fundamental principles of flow and heat transfer, some of the boundary issues are modeled using empirical data which are not necessarily appropriate for the catalytic coupling fixed-bed application and a coupling reaction kinetic model is also incorporated into the CFD model. In addition, as described earlier, the plant data regarding the fixed-bed reactor from Xu et al. (2010) are shown in Fig. 2, and also used to validate our model suggested in this work.

Table 4
Model parameters (Meng, 2003; Shackelford et al., 2002).

Descriptions	Values
Thermodynamic and physical parameters	
Gas mixture	
$C_{p,g}$ (kJ/(kmol K))	"mixing law"
ρ_g (kg/m^3)	"idea gas"
μ_g Viscosity(Pa s)	1.72×10^{-4}
k_g(W/(m K))	0.0254
$D_{i,m}$ (m^2/s)	2.393e-5
Solid phase	
$C_{P,s}$(kJ/(kmol K))	774
ρ_b(kg/m^3)	980
d_p (m)	4×10^{-3}
k_s (W/(m K))	0.156
ϕ porosity	0.4
Reactor parameters	
Scale (t/y)	300
Length (m)	3
Catalyst height (m)	1.5
Number of tubes	72
Tube inner (m)	0.027
Reactor pressure (Mpa)	0.2
Conduction oil temperature (K)	383
SV (h^{-1})	2000
Feed gas rate (m s^{-1})	0.798
Model parameters linking to boundary conditions	
Feed gas temperature (K)	343
b(m)	0.002
h_{gc} (W/(m^2 K))	176

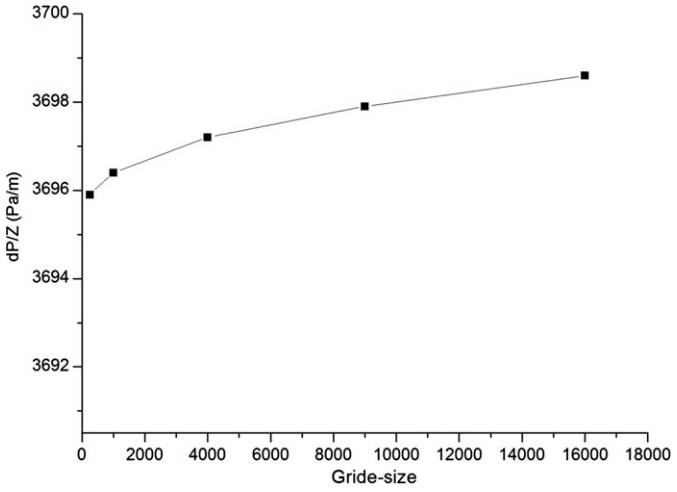

Fig. 1. Pressure drop for various mesh resolutions.

Table 5 gives the comparisons between the plant data (Xu et al. 2010) and the simulation data (one-temperature porous medium model, two-temperature porous medium model and PRO/II software simulation (Xu et al. 2010)). Table 5 shows that the simulated data using two-temperature porous medium model are in better agreement with the plant data (Xu et al., 2010) than the one-temperature porous medium model in previous analysis, when the porous medium model is applied, the default solution in Fluent software of energy equation for the porous medium is based on one-temperature model, giving only an effective thermal conductivity for the porous region. Obviously, the temperature of solid phase equals that of gas phase does not accord with the practical reactor. Therefore, the solid energy and heat transfer equations are added into the porous medium model, thus the old one-temperature porous medium model is changed into two-temperature porous medium model. The two-temperature porous medium model can predict both the temperature of gas and solid phase, as the simulation results show, the temperature of gas phase decreased nearly 6 K at the reactor out and the simulation result are more reliable.

It is found that no significant difference was observed in the predicted reaction result at the reactor out with these two kinds of flow closure model, laminar or turbulent. In general, the gas flow in the porous medium displayed low Reynolds numbers, and the effect of the turbulent behavior on the flow behavior is not very strong. Therefore, both the laminar and the turbulent models are suitable for predicting the hydrodynamic of the gas–solid flow and catalytic coupling reaction of CO–DEO in a fixed-bed reactor.

In addition, the comparison between our simulation data with the available PRO/II software simulation data is given in Table 5. Both the simulation data in this work and the PRO/II software simulation data are in good agreement with the plant data. However, the PRO/II software simulation could not inform us the axial and radial profiles of oxidation parameters in such cumbersome multiphase reaction system.

5.3. Flow field distribution in the fixed-bed reactor

When the model is verified, it is firstly used to predict the flow field in the fixed-bed reactor. In this study, we focus on the most attractive flow field described via its temperature and component distributions since the coupling reaction is a highly exothermic reaction and the produced hot spot (including its temperature

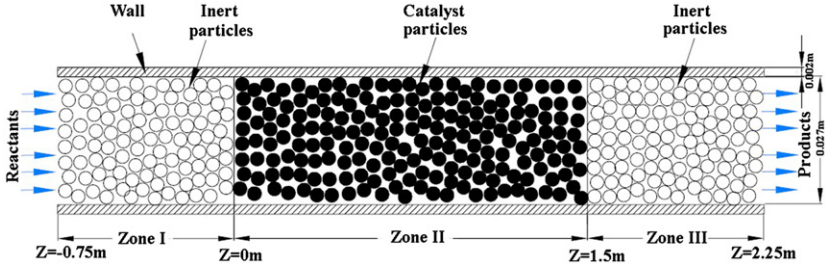

Fig. 2. Fixed-bed axial-flow reactor. Reactants enter at $Z=-0.75$ m and leave at $Z=2.25$ m. The reaction zone extends from $Z=0$ to 1.5 m.

Table 5
Comparison between the plant and the simulation data (one-temperature porous medium model, two-temperature porous medium model and PRO/II software simulation (Xu et al. 2010)).

	Coupling reactor in		Coupling reactor out					
	Plant	Simulation	Plant	One-temperature porous medium model		Two-temperature porous medium model		PRO/II software simulation
				Laminar	Turbulent	Laminar	Turbulent	
Flow rate/mol/h	118.32	118.32	121.75	120.86	120.86	120.86	120.86	121.74
temperature	378	378	405.5	412.0	411.9	406.2	406.4	405.70
Pressure/MPa	0.2	0.2	0.2	0.2	0.2	0.2	0.2	0.2
CO/molf	0.3135	0.3135	0.2440	0.2437	0.2437	0.2474	0.2474	0.2454
EN	0.1063	0.1063	0.0160	0.0114	0.0114	0.0156	0.0156	0.0170
N_2	0.5500	0.5500	0.5661	0.5632	0.5632	0.5620	0.5620	0.5658
NO	0.0047	0.0047	0.0994	0.1036	0.1035	0.0992	0.0991	0.0985
DEO	0	0	0.0435	0.0432	0.0431	0.0410	0.0410	0.0433
DEC	0	0	0.0011	0.0012	0.0012	0.0013	0.0012	0.0010
ET	0.0250	0.0250	0.0293	0.0306	0.0306	0.0305	0.0305	0.0283
H_2O	0.0005	0.0005	0.0006	0.0007	0.0007	0.0007	0.0007	0.0008

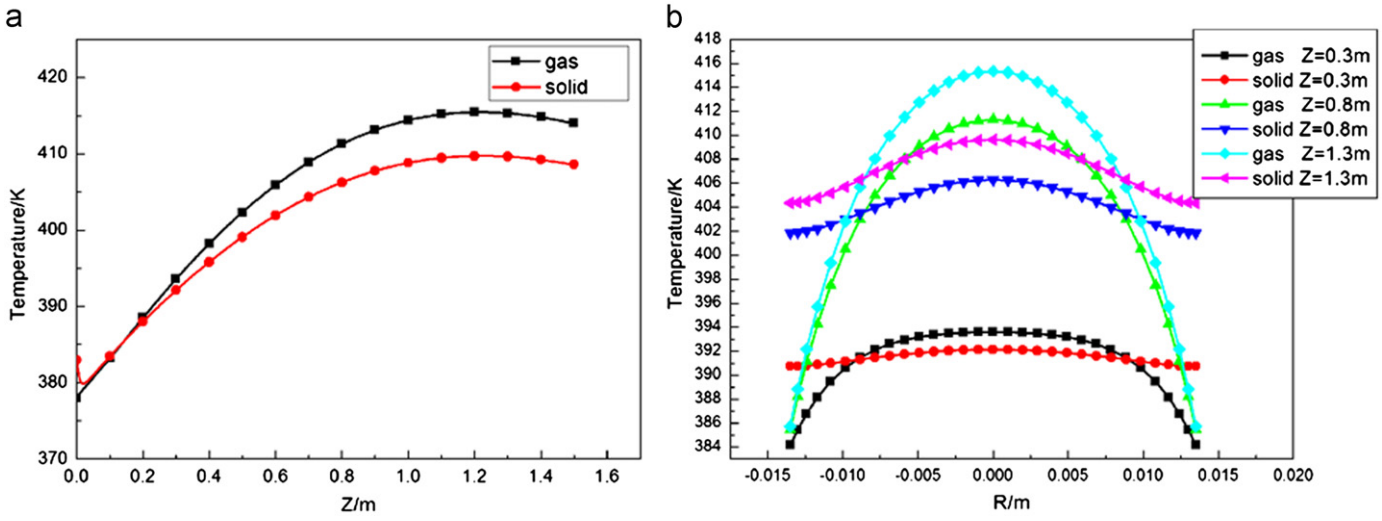

Fig. 3. Temperature profiles in the reactor. (a) Temperature distributions along axial direction of reactor and (b) temperature distributions along radial direction of reactor.

and position) strongly influences the products properties and the operational stability of fixed-bed reactor.

5.3.1. *Temperature distribution*

Fig. 3(a) and (b) shows the temperatures at different positions along the axial and radial directions, respectively. From Fig. 3(a), one knows that the hot spot locates near the exit of reactor. Before the hot spot, the solid temperature is higher than the gas temperature due to the warm-up effect of solid on the feed gas; after the hot spot, the gas temperature is higher than the solid temperature due to the heat transfer from gas to solid; near the hot spot, the gas temperature rises rapidly, while the solid temperature changes relatively slowly. From Fig. 3(b), due to the wall viscosity and heat sinking, the temperature is high in the center, low at both sides, showing a parabola shape. Before the hot spot, the solid temperature is significantly higher than the gas temperature while after the hot spot, the air temperature is higher than the solid temperature. In addition, from Fig. 3(b), there is obvious temperature change in the gas phase while only small temperature change can be observed in the solid phase. In practice, the above temperature changes are due to the much higher heat capacity and thermal conductivity performance of solid phase than those of gas phase.

5.3.2. *Component distribution*

Fig. 4(a) shows the mole fraction distribution curves of each component along the axis. Due to the chemical reactions, CO and EN are continuously consumed, when NO, DEO, and a small amount of DEC are hereby produced. Because the mole ratio of CO and EN is 3:1, EN is almost completely consumed. Fig. 4(b) is the CO mole fraction distribution curve along the radial direction, which indicates that the mole fraction distribution of CO is equally affected by the wall, presenting a parabola shape.

5.4. *Optimization study*

The operational stability and the conversion rate of the CO coupling fixed-bed reactor are mainly influenced by the inlet temperature of feed gas, coolant temperature, space velocity and inlet CO concentration. Based on the data listed in Tables 4–5, impact of each individual parameter such as temperature distribution, ethyl nitrite conversion rate and the selectivity of diethyl oxalate in the reactor are evaluated.

5.4.1. *The effect of the conduction oil temperature*

Fig. 5(a) and (b) shows the simulation results at different coolant temperatures. In Fig. 5(a), the hot spot and outlet

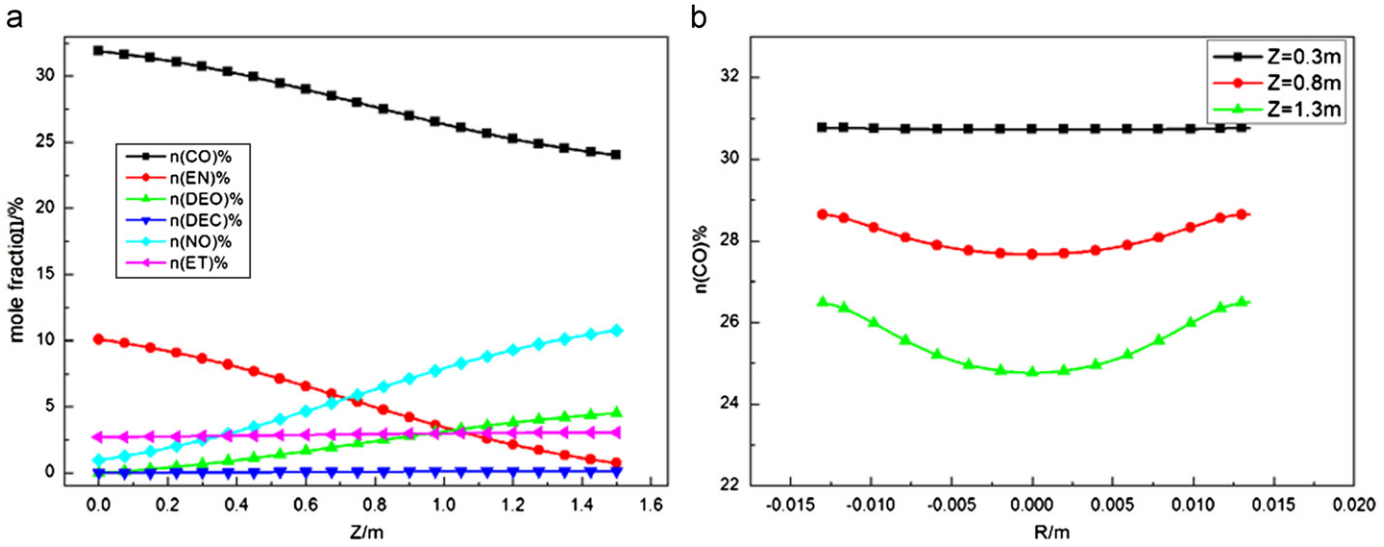

Fig. 4. Main components profiles in the reactor. (a) Mole fraction profiles of main components along axial direction of reactor and (b) mole fraction profile of CO along radial direction of reactor.

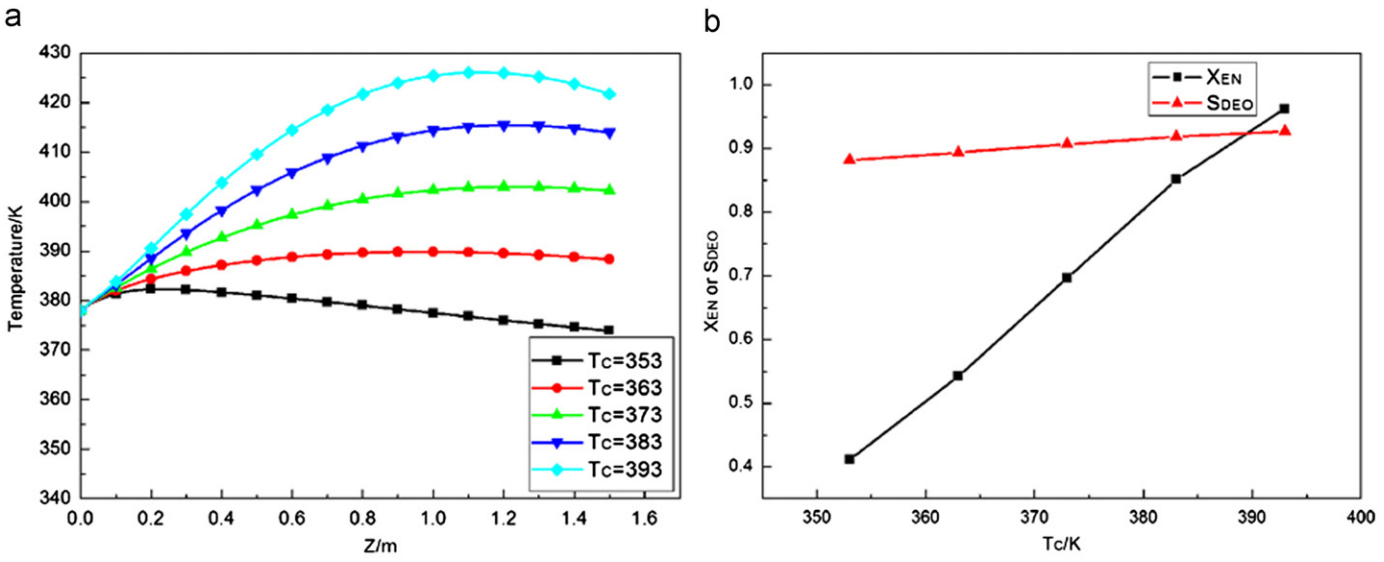

Fig. 5. The effects of coolant temperature. (a) The effect of coolant temperature on the temperature distribution along axial direction of reactor and (b) the effect of coolant temperature on the EN convenient rate and the DEO selectivity.

temperatures both increase with the increase of conduction oil temperature due to the decreased heat transfer rate, resulting in the increase of bed temperature, reaction rate and heat generation. Fig. 5(b) illustrates that the conduction oil temperature has obvious effect on the convenient rate of EN, while has no significant effect on the selectivity of DEO. Therefore, a higher conduction oil temperature can be selected if the hot spot temperature is not higher than the temperature limitation of catalyst. At the same time, the conduction oil temperature is also a sensitive factor that should be well controlled.

5.4.2. *The effect of feed gas temperature*

Fig. 6(a) and (b) shows the simulation results at different feed gas temperatures. It is known that the increase of inlet temperature of gas mixture leads to the increase of hot spot temperature and brings forward the hot spot. Moreover, the reaction rate increases with a relative higher feed gas temperature, which brings forward the reaction zones, and then at the outlet, the concentration of feed gas and heat releasing rate decreases, resulting in a slight increase in the outlet temperature. The ethyl nitrite conversion rate increases fast at outlet with the increase of feed gas temperature, while the diethyl oxalate selectivity increases slightly. As the feed gas temperature increases, which means the inlet section temperature increase, the total conversion rate of EN increases, but the activation energy of main and side reactions have little difference, which will not cause the main reaction rate increase significantly. Based on the above simulation results, we can choose the feed gas temperature from a wide range, and possibly a higher feed gas temperature if the reaction process allows.

5.4.3. *The effect of CO component*

Fig. 7(a) and (b) shows the simulation results at different molar concentrations of CO. EN must be maintained at a certain

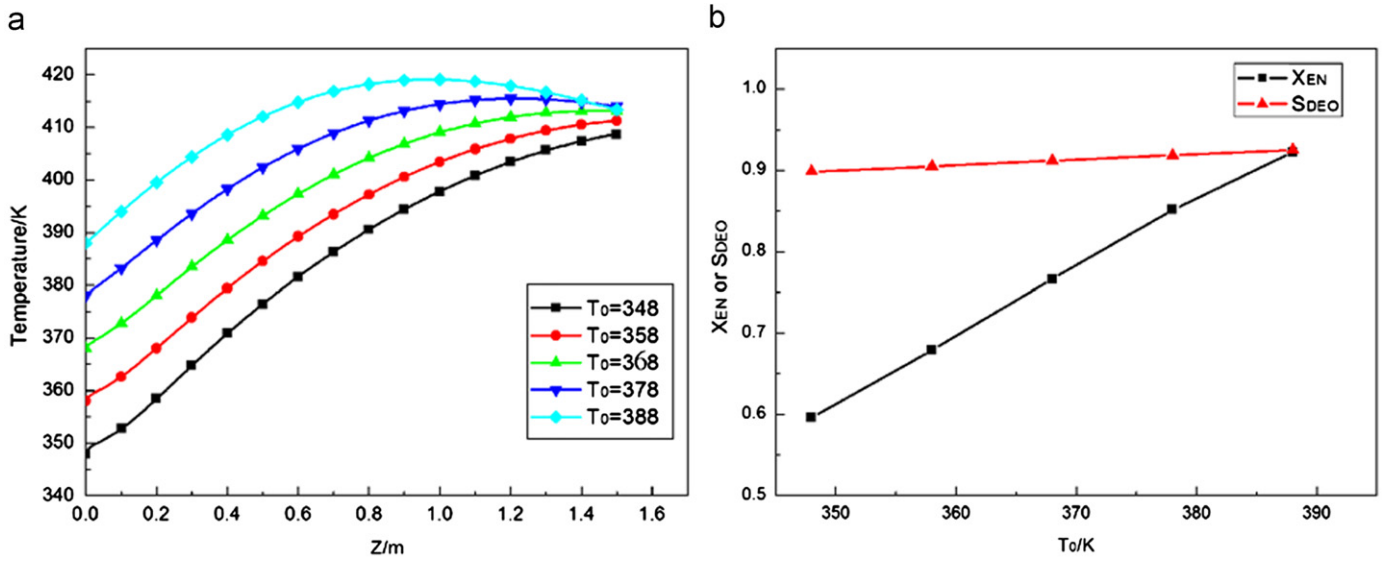

Fig. 6. The effects of feed gas temperature. (a) The effect of feed gas temperature on the temperature distribution along axial direction of reactor and (b) the effect of feed gas temperature on the convenient rate of EN and the selectivity of DEO.

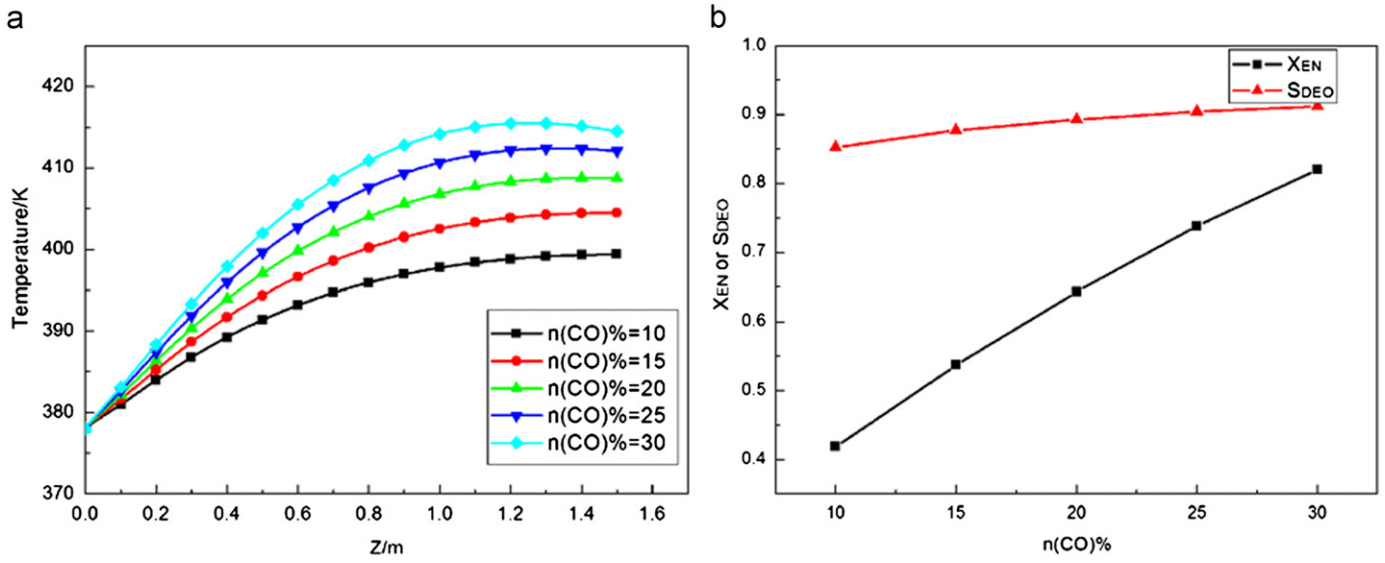

Fig. 7. The effects of CO molar concentration. (a) The effect of CO molar concentration on the temperature distribution along axial direction of reactor and (b) the effect of CO molar concentration on the EN convenient rate and the DEO selectivity.

concentration due to thermodynamic instability. The concentration of EN in feed gas is generally maintained at 10–30%. With other conditions unchanged, the temperature of hot spot increases with the increase of CO concentration, and the hot spot moves forward. In fact, one can easily find that if the concentration of EN remained unchanged, the reaction rate would increase at the entrance, which brings forward the hot spot and increases the temperature of hot spot.

The increase of CO molar concentration is helpful to increase the convention rate of EN and the selectivity of DEO. This is because EN in the reaction system decreases relatively with the increase of the CO/EN ratio, which to some extent inhibits the decomposition reaction of EN. Based on the simulation result, a more reasonable CO/EN ratio is 2–3, which not only ensure that it is not less than the main reaction stoichiometry (1:1) but also takes into account EN conversion and DEO selectivity. Therefore, CO concentration is a relatively sensitive operating parameter.

5.4.4. *The effect of space velocity*

Fig. 8(a) and (b) shows the simulation results at different space velocities. The temperature of hot spot increases with the increase of space velocity. Furthermore, the outlet temperature increases slightly, both the conversion and the selectivity of EN decrease.

In fact, when the space velocity increases, the volume flow rate of the material as well as the Reynolds number in the bed increases, resulting in the axial and radial heat transfer rate both increase, thus the radial temperature difference reduces, the hot spot temperature decreases and its position backs forward.

In addition, as the space velocity increases, the residence time of gas mixture in the reactor decreases, which results in the

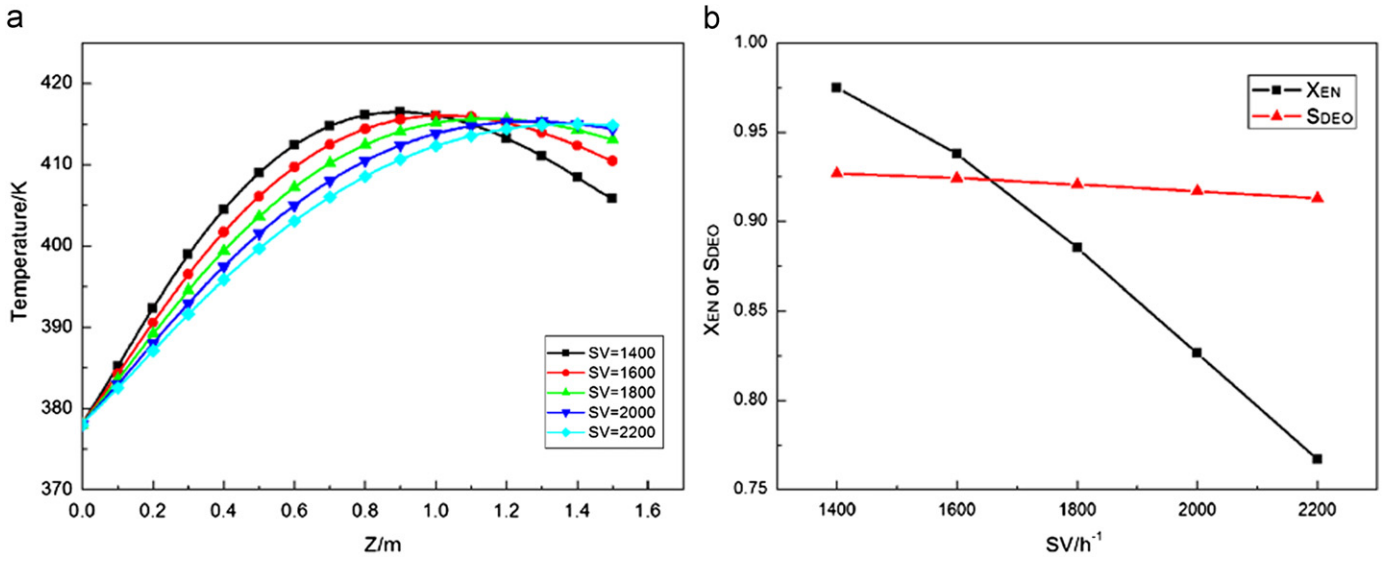

Fig. 8. The effects of space velocity. (a) The effect of space velocity on the temperature distribution along axial direction of reactor and (b) the effect of space velocity on the convenient rate of EN and the selectivity of DEO.

decrease of conversion rate. However, it will not effect on the selectivity of EN.

As described above, the reaction pressure also affects the operational performance of the reactor. However, in the CO coupling reaction, the reaction pressure is less than 0.2 MPa, basically to maintain atmospheric pressure at operation. Therefore, one does not need to consider the effect of reaction pressure. In fact, the reaction pressure is always beneficial to improve the reaction, but in this coupling reaction, the numbers of molecules variation are of small changes, thus the reaction rate is not sensitive to the increasing pressure. Therefore, there are no special requirements on the reaction pressure. According to engineering experience, desirable system pressure is 0.1–0.2 MPa.

In summary, the most sensitive operating parameters of coupling reaction are the conduction temperature and CO concentration.

5.5. Hot spot temperature analysis

For the exothermic reaction, the most critical problem is the existence of hot spot and runaway phenomena, which are paid much attention in fixed bed reactor scale-up design and operation. So it may be very useful to find out the key factor that the hot temperature mainly dictated by, since the hot spot temperature specifying is due to so many factors, including the hydrodynamic or kinetic/thermodynamic constrains of the oxidation reaction. Fig. 9 shows the sensitivity analysis of the hot spot temperature specified by changing one single parameter. The sensitivity of parameters can be listed as follows: the conduction oil temperature > the feed gas temperature > the carbon monoxide composition > the space velocity. The larger sensitivity operating parameters should be strictly controlled in the production process.

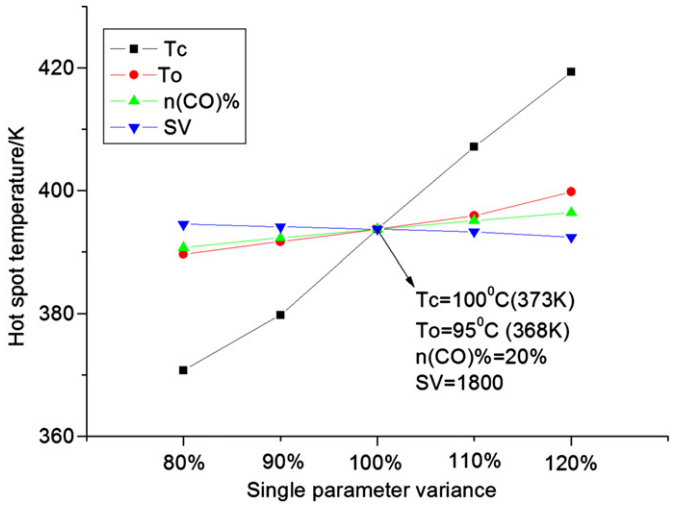

Fig. 9. The hot spot temperature sensitivity analysis.

6. Conclusions

A comprehensive two-dimensional heterogeneous reactor model was developed to simulate the flow behavior and catalytic coupling reaction of CO–DEO in a fixed-bed reactor. The solid energy and heat transfer equations are added into the porous medium model, thus the default one-temperature porous medium model was changed into two-temperature porous medium model. Comparing the results gives the following conclusions:

(1) The simulated data using two-temperature porous medium model are in better agreement with the experimental data (Xu et al., 2010) than the one-temperature porous medium model, both the laminar and the turbulent models are suitable for predicting the hydrodynamic of the gas–solid flow and catalytic coupling reaction of CO–DEO in a fixed-bed reactor.

(2) Conduction oil temperature has significant effects on the hot spot temperature of DEO synthesis reactor, while the feed gas temperature has weaker effect. The simulation results show that appropriate higher heat transfer temperature and higher feed gas temperature can be selected under the condition that the hot spots temperatures do not exceed the allowable temperature limit of the catalyst activities.

(3) The mole fraction of the feed gas CO affects the DEO selectivity and yield to a certain extent. The simulation results

show that a higher CO/EN molar ratio can be selected. A reasonable CO/EN molar ratio ranges 2.5–3.

(4) The space velocity has little effect on the reaction. To make reasonable choices of processing power of the reactor, one should consider the hot spot temperature, EN conversion rate, DEO selectivity, pressure drop and cycle power consumption.

Nomenclature

A	pre-exponential factor, kmol(kg h)
A_i	inner heat transfer area per unit length, m^2
A_m	arithmetic mean value of heat transfer area, m^2
A_O	outer heat transfer area per unit length, m^2
b	wall thickness, m
C_{b2}	constant
$C_{j,r}$	molar concentration of species j in reaction r, kmol/m^3
C_p	heat capacity at constant pressure, J/(kmol K)
d_P	catalyst particle diameter, m
$D_{i,m}$	diffusion coefficient for species i in gas mixture, m^2/s
D_b	tube inner diameter, m
E	activation energy, kJ/kmol
E_g	total energy, kg m^2/s^2
g	gravitational acceleration, m/s^2
G	entropy, kJ/(kmol K)
G_v	production of turbulent viscosity, m^2/s
h_{gc}	total heat transfer coefficient, W/(m^2 K)
h_i	species enthalpy of formation, kJ/kmol
h_v	heat transfer coefficient between gas and solid phases, W/(m^3 K)
H	enthalpy, kJ/kmol
$\bar{\bar{I}}$	identity matrix
$k_{f,r}$	forward rate constant for reaction r, units vary
M_i	symbol denoting species i
M_m	molecular weight of gas mixture, kg/kmol
$M_{w,i}$	molecular weight of species i, kg/kmol
N_r	number of chemical species in the system
Nu_v	nusselt number(dimensionless)
p	pressure, Pa
Pr	prandtl number(dimensionless)
q	heat flux, W/m^2
r	reaction rate, kmol/(kg h)
R	universal gas constant, kJ/(kmol K)
Re	reynolds number(dimensionless)
R_i	reaction rate, kg/(m^3 s)
S	gas–solid momentum exchange rate
T_c	conduction oil side temperature, K
T_g	gas mixture temperature, K
T_s	solid temperature, K
v	physical velocity vector, m/s
v^T	transpose of velocity vector, m/s
X_i	conversion of species i
y_i	mole fraction of species i
y^+	characteristic dimensionless parameter in boundary layer flow
Y_i	mass fraction of species i
Y_v	destruction of turbulent viscosity due to wall blocking and viscous damping, m^2/s^2
Z	tube length along the axils, m
α_g	fluid side heat transfer at walls, W/(m^2 K)
α_c	conduction oil side heat transfer at walls, W/(m^2 K)
ε	turbulent kinetic energy dissipation, m^2/s^3
μ	viscosity, Pa s
μ_t	turbulent viscosity, Pa s
$\tilde{\nu}$	turbulent kinematic viscosity, m^2/s
$\nu'_{i,r}$	stoichiometric coefficient for reactant i in reaction r
$\nu''_{i,r}$	stoichiometric coefficient for product i in reaction r
$\eta'_{j,r}$	rate exponent for reactant species j in reaction r
$\eta''_{j,r}$	rate exponent for product species j in reaction r
ρ_b	bulk density of bed, kg/m^3
ρ_g	density of gas mixture, kg/m^3
λ	thermal conductivity of steel, W/(m K)
k_g	thermal conductivity of gas phase, W/(m K)
k_s	thermal conductivity of solid phase, W/(m K)
$\sigma_{\tilde{\nu}}$	constant
$\bar{\bar{\tau}}$	shear stress of gas phase, pa
ϕ	porosity

Acknowledgments

The authors thank the National Natural Science Foundation of China (no. 21076171), the State-Key Laboratory of Chemical Engineering (Tsinghua University) (no. SKL-ChE-10A03) and the Fujian Province Science and Technology office of China (no. 2009HZ0005-1) for supporting this work. Authors also would like to thank the anonymous referees for comments on this manuscript.

The simulation work is implemented by advanced software tools (FLUENT 6.3.26 and GAMBIT 2.3.16) provided by the China National Petroleum Corporation and its subsidiary company.

References

Bartley, W.J., Charleston, W.V., 1987. Process for the preparation of ethylene glycol. US Patent 6 77234.

Bub, G., Baerns, M., Bussemeier, B., Frohning, C., 1980. Prediction of the performance of catalytic fixed bed reactors for Fischer–Tropsch synthesis. Chem. Eng. Sci. 33, 348–352.

Calis, H.P.A., Nijenhuis, J., Paikert, B.C., Dautzenberg, F.M., van den Bleek, C.M., 2001. CFD modeling and experimental validation of pressure drop and flow profile in a novel structured catalytic reactor packing. Chem. Eng. Sci. **56**, 1713–1724.

Chatterjee, D., Deutschmann, O., Warnatz, J., 2001. Detailed surface reaction mechanism in a three-way catalyst. Faraday Discuss. 119, 371–384.

Coussirat, M., 2001. Numerical study of turbulence models for imprinting gas–jet systems. von Karman Institute for Fluid Dynamics, Internal Report VKI-PR 2001-05.

Durbin, P.A., Petterson, B.A., 2001. Statistical Theory and Modeling for Turbulent Flows. Wiley, New York, pp. 138-139.

Ding, J., Gidspow, D., 1990. A bubbling fluidization model using kinetic-theory of granular flow. AIChE. J. 36, 523–531.

Eu Toit, C.G., Rousseau, P.G., Greyvenstein, G.P., Landman, W.A., 2006. A systems CFD model of a packed bed high temperature gas-cooled nuclear reactor. Int. J. Therm. Sci. 45, 70–85.

Ergun, S., 1952. Fluid flow through packed columns. Chem. Eng. Prog 48, 89–94.

Eugene, M.G., Andre, V.K., 2001. Carboxylates in catalytic hydrolysis of alkylene oxides. US Patent 6, 316, 571.

Gao, X., Shi, D.P., Chen, X.Z., Luo, Z.H., 2010. Three-dimensional CFD model of the temperature field for a pilot-plant tubular loop polymerization reactor. Powder Technol. 203, 574–590.

Gao, Z.H., Liu, Z.C., He, F., Xu, G.H., 2005. Combined XPS and in situ DRIRS study of mechanism of Pd–Fe/α-Al_2O_3 catalyzed CO coupling reaction to diethyl oxalate. J. Mol. Catal. A: Chem 235, 143–149.

Guardo, A., Coussirat, M., Larrayoz, M.A., Recasens, F., Egusquiza, E., 2004. CFD flow and heat transfer in nonregular packings for fixed bed equipment design. Ind. Eng. Chem. Res. 43, 7049–7056.

Guardo, A., Coussirat, M., Larrayoz, M.A., Recasens, F., Egusquiza, E., 2005. Influence of the turbulence model in CFD modeling of wall-to-fluid heat transfer in packed beds. Chem. Eng. Sci. 60, 1733–1742.

Guardo, A., Coussirat, M., Recasens, F., Larrayoz, M.A., Escaler, X., 2006. CFD study on particle-to-fluid heat transfer in fixed bed reactors: Convective heat transfer at low and high pressure. Chem. Eng. Sci. 61, 4341–4353.

Henneke, M.R., Ellzey, J.L., 1999. Modeling of filt ration combustion in a packed bed. Combust. Flame 117, 832–840.

Jafari, A., Zamankhan, P., Mousavi, S.M., Pietarinen, K., 2008. Modeling and CFD simulation of flow behavior and dispersivity through randomly packed bed reactors. Chem. Eng. J. 144, 476–482.

Jakobsen, H.A., Lindborg, H., Handeland, V., 2002. A numerical study of the interactions between viscous flow, transport and kinetics in fixed bed reactors. Comput. Chem. Eng. 26, 333–357.

Jess, A., Popp, R., Hedden, K., 1999. Fischer–Tropsch synthesis with nitrogen-rich syngas: Fundamentals and reactor design aspects. Appl. Catal. A-Gen. 186, 321–342.
Jiang, Y., Khadilkar, M.R., Al-Dahhan, M.H., Dudukovic, M.P., 2001. CFD modeling of multiphase flow distribution in catalytic packed bed reactors: scale down issues. Catal. Today. 66, 209–218.
Ji, Y., Liu, G., Li, W., Xiao, W.D., 2009. The mechanism of CO coupling reaction to form dimethyl oxalate over Pd/α-Al_2O_3. J. Mol. Catal. A: Chem. 314, 63–70.
Lan, X.Y., Xu, C.M., Wang, G., Wu, L., Gao, J.S., 2009. CFD modeling of gas–solid flow and cracking reaction in two-stage riser FCC reactors. Chem. Eng. Sci. 64, 3847–3858.
Launder, B.E., Spalding, D.E., 1974. The numerical computation of turbulent flows. Comput. Methods Appl. Mech. Eng. 3, 269–289.
Le Gall, N., Luart, D., Salaun, J.Y., des Abbayes, H., Toupet, L., 2001. Mechanism of formation of the metallacyclic iron carbenes (CO)(3)Fe[=C(NR2)OC(O)NR2] formed by thermal evolution of bis carbamoyl complexes, characterization of eta(2)-carbamoyl intermediates. J. Organomet. Chem. 617, 483–494.
Li, Y.C., He, W.J., Fui, T.K., 2005. The method for production of ethylene glycol via direct catalytic hydrolysis of ethylene oxide over solid catalyst. CN Patent 1566 049.
Li, Z.H., He, C.Y., Yin, D.X., Wang, B.W., Xu, G. H., M.A.X.B., 2005. Macrokinetics of CO catalytic coupling reaction to produce diethyl oxalate. J. Chem. Ind. Eng. 56, 2314–2319 in Chinese.
Lopes, R.J.G., Quinta-Ferreira, R.M., 2010a. Evaluation of multiphase CFD models in gas–liquid packed-bed reactors for water pollution abatement. Chem. Eng. Sci. 65, 291–297.
Lopes, R.J.G., Quinta-Ferreira, R.M., 2010b. Assessment of CFD Euler–Euler method for trickle-bed reactor modelling in the catalytic wet oxidation of phenolic waste waters. Chem. Eng. J. 160, 293–301.
Meng, F.D., 2003. Process analysis and simulation for the catalytic coupling reaction of carbon monoxide to diethyl oxalate. Ph.D. Dissertation, Tianjing University, Tianjing, China.
Natarajan, S., Zhang, C., Brien, S., 2005. Numerical simulation and experimental verification of gas flow through packed beds. Powder Technol. 152, 31–40.
Nijemeisland, M., Dixon, A.G., 2001. Comparison of CFD simulations to experiment for convective heat transfer in a gas–solid fixed bed. Chem. Eng. J. 82, 231–242.
Nijemeisland, M., Dixon, A.G., 2004a. CFD study of fluid flow and wall heat transfer in a fixed bed of spheres. AIChE J. 50, 906–921.
Nijemeisland, M., Dixon, A.G., Stitt, E.H., 2004b. Catalyst design by CFD for heat transfer and reaction in steam reforming. Chem. Eng. Sci. 59, 5185–5191.
Nikačević, N.M., Petkovska, M., Duduković, M.P., 2009. Solids flow pattern in gas-flowing solids-fixed bed contactors. Part II Mathematical modeling. Chem. Eng. Sci. 64, 2491–2500.
Petre, C.F., Larachi, F., Iliuta, I., Grandjean, B.P.A., 2003. Pressure drop through structured packings: breakdown into the contributing mechanism by CFD modeling. Chem. Eng. Sci. 58, 163–177.
Qian, B.Z., 2009. The industrialization of the preparation technology of ethylene glycol based on coal in China. Petrochem. Technol. Appl. 27, 360 in Chinese.
Shackelford, J., Alexande, W., Pork, J.S., 2002. CRC Materials Science and Engineering Handbook. CRC Press Inc., New York, US, pp. 1-237.
Shiomi, Y.H., Matsuzaki, T., Masunaga, K., 1989. Process for the preparation of a diester of oxalic acid. US Patent 4874888.
Shoaeifar, P., Abbasian, M., Entezami, A.A., 2007. A convenient method for preparation of amphiphilic monomethoxypoly(ethylene glycol)-polystyrene diblock copolymer by NMRP technique. J. Polym. Res. 14, 45–52.
Spalart,P., Allmaras, S., 1992.A one-equation turbulence model for aerodynamic flows. Technical Report, American Institute of Aeronautics and Astronautics, AIAA-92-0439.
Taskin, M.E., Dixon, A.G., 2008. CFD study of the influence of catalyst particle design on steam reforming reaction heat effects in narrow packed tubes. Ind. Eng. Chem. Res., 5966–5975.
Tian, Z.F., Tu, J.Y., Yeoh, G.H., 2007a. CFD studies of indoor airflow and contaminant particle transportation. Particul. Sci. Technol. 25, 555–570.
Tian, Z.F., Tu, J.Y., Yeoh, G.H., 2007b. Numerical modelling and validation of gas-particle flow in an in-line tube bank. Comput. Chem. Eng. 31, 1064–1072.
UOPLLC., 2002. Attrition resistant catalyst for light olefin production. WO PCT 05952A2.
Wakao, N., Kaguei, S., 1982. Heat and Mass Transfer in Packed Beds. Gordon and Breach Science Publishers, New York, US, pp. 23-102.
Wang, B.W., Ma, X.B., Mao, L.F., Xu, G.H., 2000. Simulation of the process of diethyl oxalate prepared by CO coupling-regeneration reaction. J. Nat. Gas Chem. 9, 187–196.
Wu, Q., Cao, Z.H., He, F., Xu, G.H., 2003. Influence of oxygen on activity of Pd–Fe/alpha-Al_2O_3 catalyst for CO coupling reaction to diethyl oxalate. Chin. J. Catal. 24, 289–293.
Xiao, W.J., Vasapollo, G., Alper, H., 2000. Highly regioselective thiocarbonylation of conjugated dienes via palladium-catalyzed three-component coupling reactions. J. Org. Chem. 65, 4138–4144.
Xu, G.H., Ma, X.B., He, F., Chen, H.F., 1995. Characteristics of catalyst for carbon monoxide coupling reaction. Ind. Eng. Chem. Res. 34, 2379–2382.
Xu, G.H., Ma, X.B., Wang, B.W., Li, Z.H., Zhang, Y.M., 2008a. The method for production of diethyl oxalate via carbon monoxide coupling reaction. CN Patent 101143821.
Xu, Y., Ma, X.B., Li, Z.H., 2008b. Simulation analysis on tube–shell type fixed bed reactor for synthesis of diethyl oxalate in gaseous phase. Chem. React. Eng. Technol. 24, 204–210 in Chinese.
Xu, Y., Li, R., Chen, M.M., Ma, X.B., 2010. Simulation of synthesizing diethyl oxalate by gaseous phase coupling carbon monoxide and ethyl nitrite. J. Chem. Eng. Chin. Univ. 24, 209–213.
Zhang, B.K., Guo, T.H., Huang, C.P., Wang, J.M., 1995. Catalyst for production of diethyl oxalate. CN Patent 95116139.